

# Role of Lubrication Oil in Particulate Emissions from a Hydrogen-Powered Internal Combustion Engine

ARTHUR L. MILLER,<sup>\*,†</sup>  
CHRISTOPHER B. STIPE,<sup>‡</sup>  
MATTHEW C. HABJAN,<sup>†,§</sup> AND  
GILBERT G. AHLSTRAND<sup>||</sup>

National Institute for Occupational Safety and Health,  
Spokane, Washington 99207 Mechanical Engineering  
Department, Seattle University, Seattle, Washington 98122,  
Mechanical Engineering Department, Gonzaga University,  
Spokane, Washington 99258, and College of Biological  
Sciences Imaging Center, University of Minnesota,  
St. Paul, Minnesota 55108

Recent studies suggest that trace metals emitted by internal combustion engines are derived mainly from combustion of lubrication oil. This hypothesis was examined by investigation of the formation of particulate matter emitted from an internal combustion engine in the absence of fuel-derived soot. Emissions from a modified CAT 3304 diesel engine fueled with hydrogen gas were characterized. The role of organic carbon and metals from lubrication oil on particle formation was investigated under selected engine conditions. The engine produced exhaust aerosol with log normal-size distributions and particle concentrations between  $10^5$  and  $10^7$   $\text{cm}^{-3}$  with geometric mean diameters from 18 to 31 nm. The particles contained organic carbon, little or no elemental carbon, and a much larger percentage of metals than particles from diesel engines. The maximum total carbon emission rate was estimated at  $1.08 \text{ g h}^{-1}$ , which is much lower than the emission rate of the original diesel engine. There was also evidence that less volatile elements, such as iron, self-nucleated to form nanoparticles, some of which survive the coagulation process.

## 1. Introduction

Evidence suggests that particulate matter produced in internal combustion engines results in harmful health effects (1, 2). The causal mechanisms have not been clearly identified, and it is possible that trace metals or metal-bearing ultrafines may play a role (3, 4). Therefore, it is critical to understand the origin and fate of metals and the physical processes related to nanoparticle formation in engines. Previous research focused on the origin and fate of metals during diesel engine combustion (5, 6). This study expands on that research by generating particles under conditions where soot availability is very low.

It is well documented that internal combustion engines produce soot particles during the combustion process (7, 8).

\* Corresponding author phone: (509) 354-8028; fax: (509) 354-8099; e-mail: ALMiller@cdc.gov.

<sup>†</sup> National Institute for Occupational Safety and Health.

<sup>‡</sup> Seattle University.

<sup>§</sup> Gonzaga University.

<sup>||</sup> University of Minnesota.

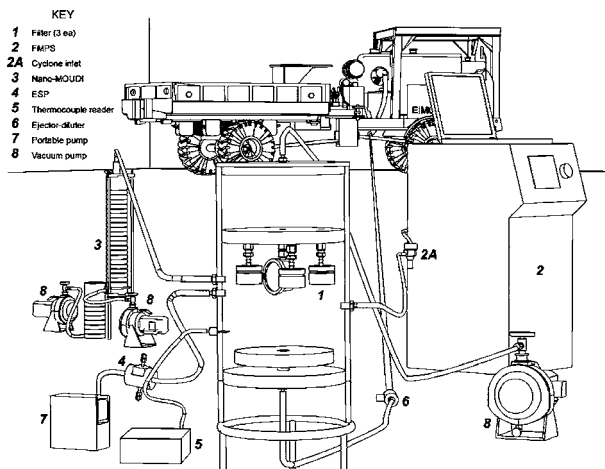


FIGURE 1. Hydrogen-powered vehicle and experimental setup.

Soot particles provide significant surface area for interaction with other combustion byproducts, including organic compounds, ash, and metals (9, 10). Earlier studies of engine emissions often focused on the relative amount of elemental and organic carbon emitted because both are derived from the combustion of hydrocarbon fuels and oils. More recently, studies have focused on the contribution of lubrication oil to the particle-formation process (11) and, in particular, the role of lubrication oil additives in particle formation (5, 12).

Under normal diesel engine operation, trace metals are vaporized and adsorbed or condensed onto the surface of soot particles (5). The origin of the metals may be from trace metals in the fuel or from the metallic fuel additives in the fuel used for diesel particulate filter regeneration. However, more typically, the metals in exhaust particles originate from lubrication oil that is spread onto the cylinder walls by the piston rings or that enters the combustion chamber via reverse blow-by of the rings (13). This is evidenced by data showing measurable levels of metallic lube oil additives in bulk diesel particulate matter (DPM) samples (14). Other recent data demonstrate a correlation between the mass of calcium and organic carbon (OC) in bulk particulate samples because of their common origin in the lubrication oil (15). The latter is consistent with previous diesel particulate data showing that OC is derived from hydrocarbons associated with lubrication oil (11). In diesel engines, the combustion of lubrication oil contributes to particle formation by increasing the amount of semivolatile hydrocarbon species available for nucleation upon exiting the tailpipe. In addition, the (metallic) ash residues combine with soot particles, and in some cases where the metal-to-carbon ratio is high, metal vapors self-nucleate inside of the engine to form a population of metal-rich nanoparticles (5, 16).

The primary goal of this study was to investigate the formation of combustion-generated particles derived from lubrication oil in the absence of fuel-produced soot. This was accomplished by an examination of the emissions from a hydrogen-fueled internal combustion engine because it does not produce fuel-derived soot during the combustion process. This study's findings may increase current knowledge about the role of lubrication oil in particle-formation dynamics as engine technology improves and cleaner internal combustion engines are developed. The results are not meant to be used in direct comparison with other engine types but rather to demonstrate the formation of particles derived solely from lubrication oil. The secondary goal was to study how

the number concentration and size distribution of the lubrication-oil-derived particles depend on the engine loading condition. This goal is of particular significance because, in 2008, the Mining Safety and Health Administration (MSHA) plans to phase in a final particulate matter rule limiting exposure of metal and nonmetal underground miners to 160  $\mu\text{g m}^{-3}$  of total carbon (TC) (17). In addition, the current regulated limit for particulate matter emission by any underground source in underground coal mines is 2.5  $\text{g h}^{-1}$  (18). Presently, many approaches, including particulate filters and low sulfur fuels, are being considered to achieve the regulated limits; this study investigated the viability of hydrogen-powered engines to achieve the regulated levels of particulate matter.

## 2. Experimental Procedure

The experiment was conducted using a CAT 3304 engine which had been modified to burn hydrogen gas. In its normal configuration, this engine is a 7-liter, 85-HP, 4-cylinder diesel engine. Modifications included equipping the engine with a spark ignition system, lowering the compression ratio, turbo charging, and adding an aftercooler and a parallel fuel-induction system (19). The engine was installed in an EIMCO model 975 mine utility vehicle called the Zero Emission Utility Solution or “ZEUS” (20). Recently, the ZEUS was employed in the first demonstration of a hydrogen-fueled internal combustion engine vehicle in an underground mine at the Stillwater Mine in Nye, Montana (21, 22).

During our study, emissions were monitored under three engine-operating conditions: low idle, torque stall, and high load. To attain the high load condition, the vehicle was run on a chassis dynamometer at wheel loading of 28 hp, although the actual engine load was greater because of differential and transmission friction. The low idle and torque stall tests were conducted without the aid of the dynamometer to simulate typical conditions for field testing of mining vehicles (23, 24). The torque stall was initiated by shifting the vehicle into high gear, setting the brakes and depressing the acceleration pedal manually to maintain 1500 rpm.

For all tests, a portion of the raw exhaust was cooled and diluted using an ejector-type dilutor (25). The dilution ratio was cold-flow calibrated to be approximately 10:1. The diluted aerosol was routed to a multiport sampler (Figure 1), which provided a common source of well-mixed and aged aerosol for concurrent measurements with multiple instruments. The multiport sampler consisted of a baffle to spread and mix the incoming air, a plenum (sampling) chamber, and a vacuum chamber. The two chambers were separated by a sealing plate in which multiple critical orifices were installed to provide controlled flow for instruments and filter samples. Additional sampling ports were located in the walls of the plenum. A gauge was connected to the vacuum chamber and monitored to ensure critical flow through the orifices, while the aerosol temperature was monitored at both the tailpipe and in the multiport sampler. The residence time of the particles in the sampling system was approximately 15 s.

**2.1. Measurement and Analysis Methods.** The emitted particulate matter was measured and characterized using four measurement approaches, based on the following characteristics of the particulate matter: particle number concentrations and size distributions, elemental and organic carbon concentrations, particle morphology, and particle elemental chemical composition. The instrument setup is depicted in Figure 1. The instrumentation and the purpose of each measurement technique are described in the following sections.

**2.1.1. Particle Number Concentrations and Size Distributions.** Number-weighted particle size distributions were measured using a fast mobility particle sizer (FMPS Model

**TABLE 1. Summary of Number Concentration (NC) and Particle Size for Three Engine Conditions**

	mean NC (particles $\text{cm}^{-3}$ )	RSD (%)	geometric mean mobility diameter (nm)	exhaust gas temp ( $^{\circ}\text{C}$ )	mean engine speed (RPM)	EC ( $\text{mg m}^{-3}$ )	OC ( $\text{mg m}^{-3}$ )
low idle	$2.5 \times 10^5$	4.3	31	150	800	0.027	0.404
torque stall	$3.5 \times 10^6$	23.7	19	315	1500	0.173	1.55
high load	$7.7 \times 10^6$	12.1	18	345	1900	0.310	2.87

3091, TSI Inc, St. Paul, MN). The FMPS incorporates multiple electrometers along the length of a differential mobility analyzer (DMA) (26). The DMA size-selects the particles according to electric mobility diameter, and the electrometers measure the number concentration at each size simultaneously. A particle size distribution was obtained every second during the tests within the 5.6–560 nm range. The FMPS inlet was connected to the multiport sampler, and it extracted a flow of 10  $\text{L min}^{-1}$  continuously. A cyclone with a designed cutoff of 1.0  $\mu\text{m}$  was installed at the inlet to remove particles that were much larger than the range of detection.

**2.1.2. Elemental and Organic Carbon Concentrations.** The mass concentration of elemental and organic carbon (EC and OC) in the exhaust aerosol was derived from filter samples using the NIOSH standard method 5040 (27), modified slightly with respect to sampling flow rate. Samples were collected on 37 mm prebaked quartz filters mounted in plastic cassettes. To maximize the mass of particulate for the relatively short tests (approximately 20–30 min), the flow rate through the filters was set at 22.1  $\text{L min}^{-1}$  for all tests, using a critical orifice in line with the filter cassette in the multiport sampler. A filter sample was collected for each test, and the values for EC and OC were derived from analytical results (Table 1).

**2.1.3. Particle Morphology.** Particle morphologies were determined using transmission electron microscopy (TEM) to image samples collected on 3 mm diameter, silicone monoxide-filmed grids. Most samples were collected using an electrostatic precipitator (ESP), which was built in-house and modeled after the Rochester design (28). The ESP was connected to the multiport sampler, and the flow was supplied by a GilAir5 pump (Sensidyne Inc, Clearwater, FL) at approximately 1  $\text{L min}^{-1}$ . Samples collected in this way offer a representative picture of the various particle morphologies and their relative frequency of occurrence, albeit biased toward the larger sizes because of the size-dependent charging efficiency of the ESP. In addition, samples were also collected by attaching TEM grids onto the latter five stages of a 13-stage micro-orifice uniform deposition impactor (NanoMOUDI, MSP, Shoreview, MN).

**2.1.4. Particle Elemental Chemical Composition.** The ESP and MOUDI samples were also used to investigate the elemental composition of the various particle types using a combination of TEM and energy-dispersive spectroscopy (EDS). The following protocol, designed to be performed manually by a microscopist, was developed to qualitatively characterize the aerosol from a TEM grid sample: (1) Select areas of the TEM grid and tabulate the size and morphology of all particles in the designated area. (2) Identify “typical” particle morphologies using this tabulated information. (3) Estimate/count the prevalence of each particle type. (4) Analyze several particles of each type using EDS and combine the spectra using a qualitative technique (see section 3.4) to approximate the elemental composition for each morphology type. (5) Choose a typical particle of each type and create a high magnification TEM image and an EDS spectrum for that particle.

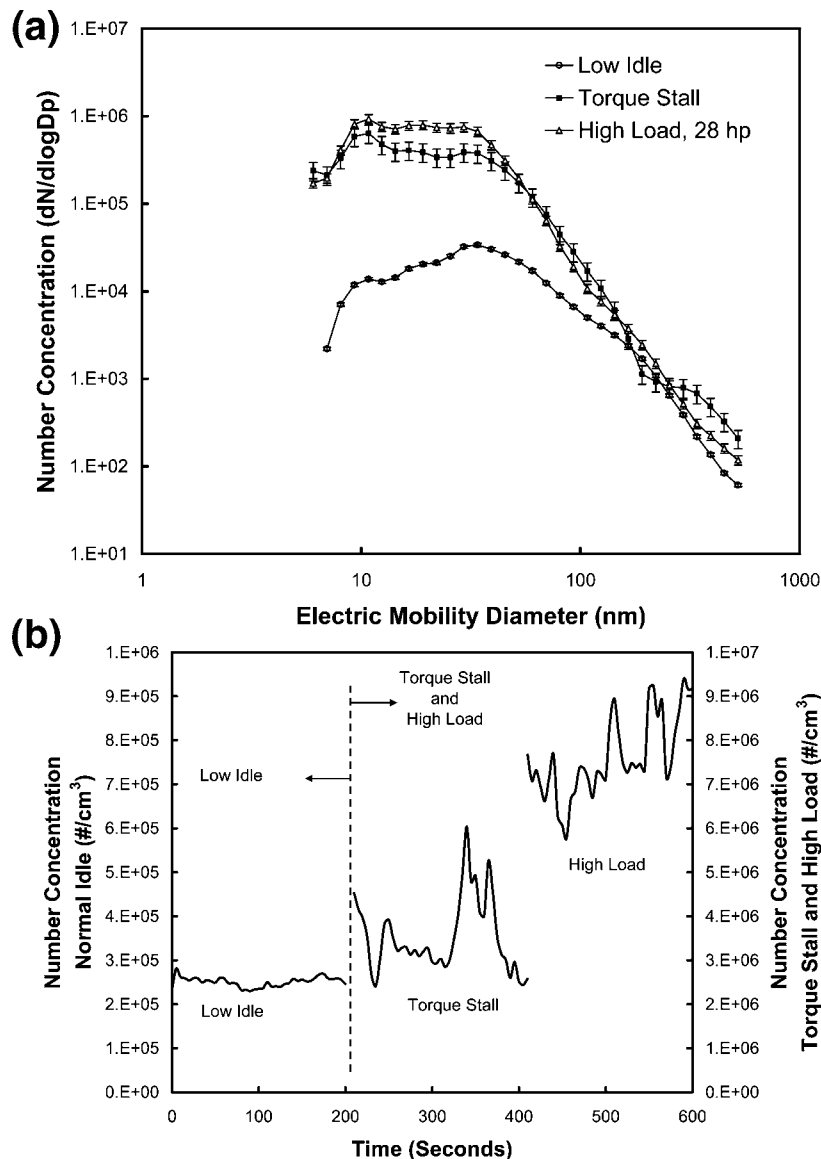


**FIGURE 2. Three engine conditions were evaluated: low idle, torque stall, and high load at 28 hp. (Note that actual engine load is greater because of differential and transmission friction.) (a) Representative particle size distributions for each condition. (b) Number concentrations over time (after 10 min engine warm-up) for each condition.**

It is important to note that this protocol is not meant to be robustly quantitative; rather, it is a simple and quick qualitative characterization of the sampled aerosol. All grid samples were analyzed using a FEI CM12 TEM with EDAX Power MX EDS capability. Background-corrected spectra were obtained by subtraction of the substrate support film background spectra from particle spectra.

### 3. Results and Discussion

The results of the analyses are presented here in four subsections that correspond to the four analysis methods outlined in the previous sections. The test results for each of the three engine conditions are summarized in Table 1.

**3.1. Particle Number Concentrations and Size Distributions. Low Idle.** At the low idle condition, the engine emitted  $2.5 \times 10^5$  particles  $\text{cm}^{-3}$  (the RSD calculated from multiple FMPS measurements was  $\pm 4.3\%$ ), with a geometric mean mobility diameter of 31 nm (Figure 2a and b). The number concentrations measured by the FMPS were corrected for the 10:1 dilution of the engine exhaust. The size distribution for the low idle condition is given in

Figure 2a, and the time-dependent number concentration for the low idle engine condition is shown in Figure 2b. The average number concentrations and mean electric mobility diameters for all engine conditions are given in Table 1. The diameter, number concentration, and mass concentration of particles for all engine loading conditions are significantly smaller than for a diesel engine, mainly because of the lack of soot agglomerates and fuel-derived particles. However, the number concentration of particles is still substantial.

**3.1.1. Torque Stall.** Particle concentrations for the torque stall condition (Figure 2b) were less stable than the other cases, which was partly caused by the inability of the operator to hold the throttle constant. Normally, an engine torque stall is performed at the maximum throttle setting, but because this engine has a governor-triggered safety switch to prevent excess revving, the researchers attempted to hold the throttle pedal manually at an intermediate setting to maintain the engine at 1500 rpm. The average number concentration of particles produced by this condition was  $3.5 \times 10^6$  particles  $\text{cm}^{-3}$  (RSD = 23.7%) with a geometric mean electric mobility diameter of 19 nm.

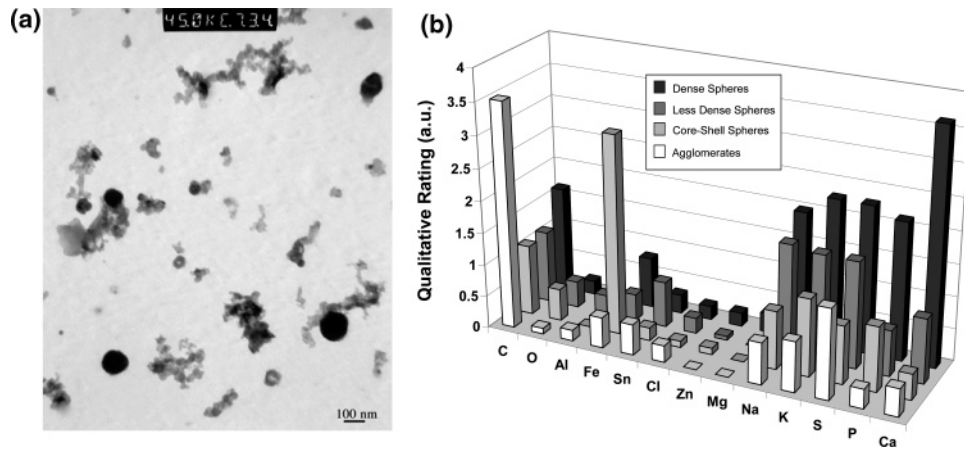


FIGURE 3. (a) TEM image of grid sample shows the range in size and type of particles. (b) Histograms of average rated spectra for four different particle types. The  $\gamma$ -axis represents the qualitative rating scheme described in the text.

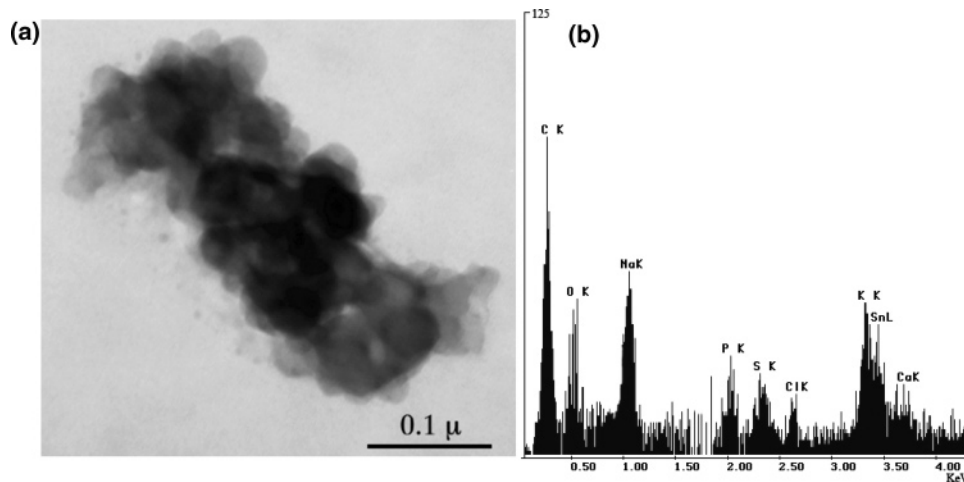


FIGURE 4. Agglomerate particle: (a) TEM image and (b) EDS spectrum of this particle showing high C content.

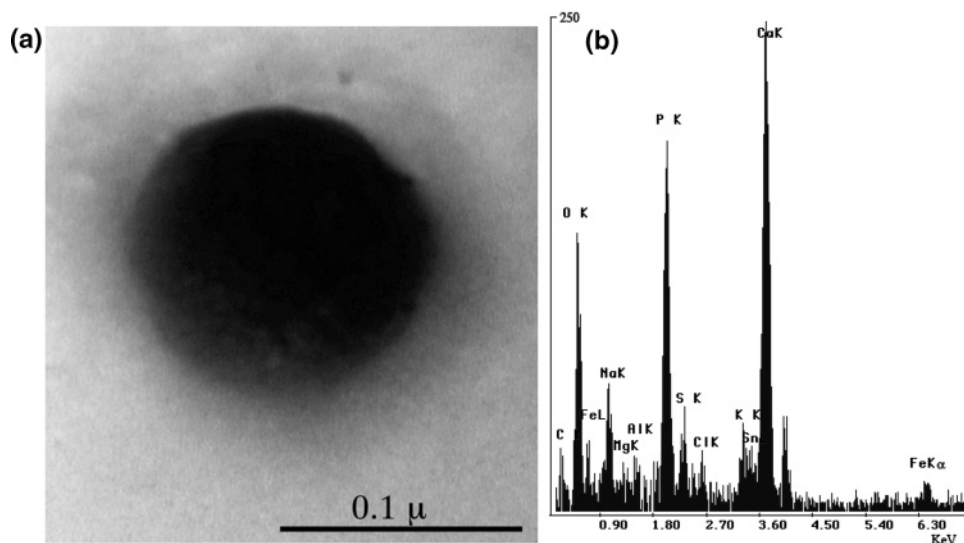


FIGURE 5. Dense sphere particle: (a) TEM image and (b) EDS spectrum of this particle showing metals derived from lubrication oil additives.

3.1.2. High Load. The average number concentration for the high load conditions was  $7.7 \times 10^6$  particles  $\text{cm}^{-3}$  (RSD = 12.1%) (Figure 2b), and the geometric mean electric mobility diameter was approximately 18 nm. The particle concentrations emitted under engine load were more scat-

tered than for the low idle condition. The greater deviation at high load was most likely the result of the unsteadiness of the engine operation on the dynamometer. Since the throttle was controlled manually with a foot pedal, there were variations over time in the engine rpm (and thus applied

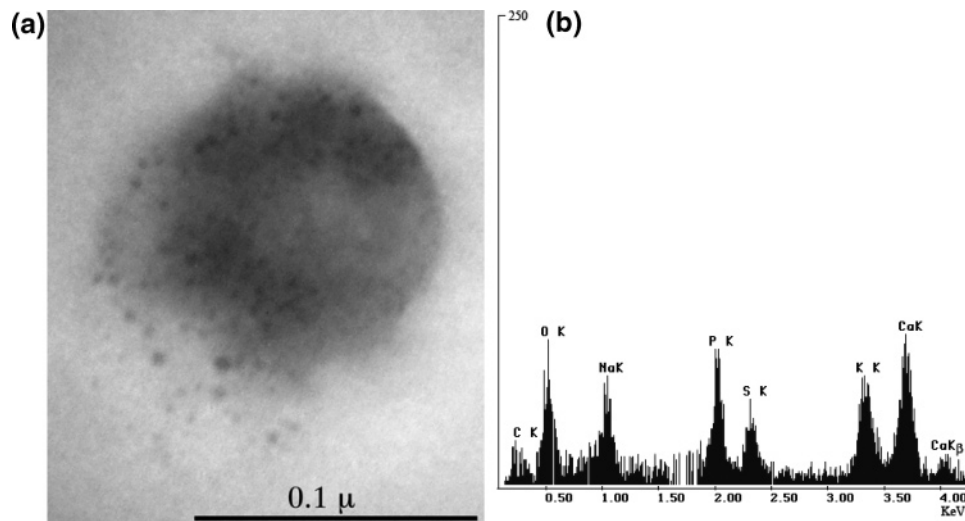


FIGURE 6. Less-dense sphere particle: (a) TEM image and (b) EDS spectrum of this particle showing trace metals from lubrication oil.

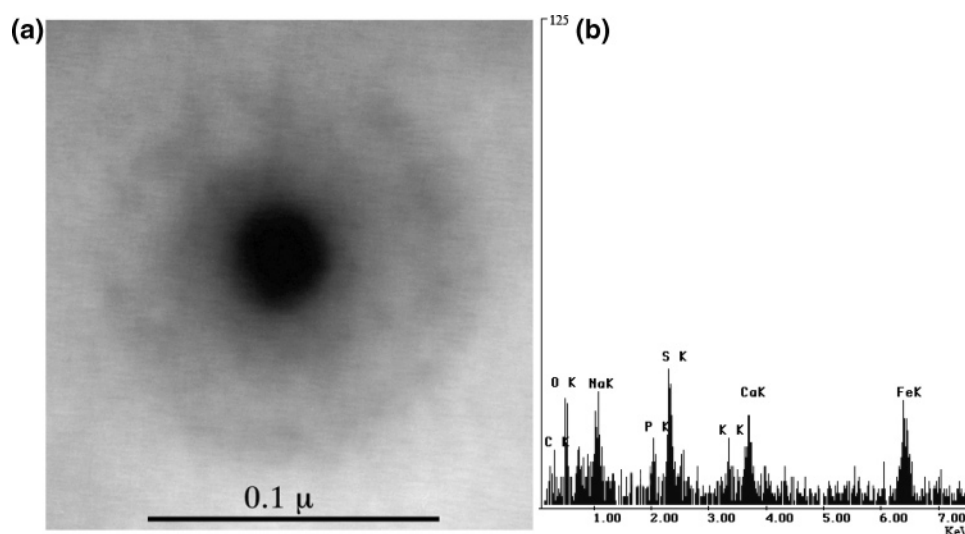


FIGURE 7. Core-shell particle with dense core: (a) TEM image and (b) EDS spectrum showing Fe, Ca, and other metals similar to dense spheres.

load) and exhaust gas temperature, which both affect particle concentration.

**3.2. Elemental and Organic Carbon Concentrations.** No fuel-derived soot forms during hydrogen combustion; therefore, the mass concentration of EC measured in the exhaust was relatively low (Table 1). This was expected because the formation of primary particles of elemental carbon (soot) typically takes place inside a flame where carbon-based fuels are burned (29). In contrast, the carbon measured in our tests was concluded to be derived from the lubrication oil. Furthermore, the EC/OC ratio increased at high load, suggesting that the higher temperatures in the cylinder resulted in the more complete breakdown of the carbon from the oil. The evidence that carbon from the lubrication oil is mostly emitted as OC further confirmed the work of Sakurai et al. (11). Emissions of organic carbon were comparable to a diesel engine of similar size (30), while elemental carbon emissions were extremely low.

The maximum total carbon emission rate for this engine was  $1.08 \text{ g h}^{-1}$  at the high load condition, assuming a volumetric engine efficiency of 85%. This is much smaller than the  $30 \text{ g h}^{-1}$  of diesel particulate matter emitted from the original CAT 3304 diesel engine and is also less than the  $2.5 \text{ g h}^{-1}$  limit noted in the recent MSHA regulation (18).

**3.3. Particle Morphology.** To study the morphology and chemical composition of particles emitted by this engine,

TEM/EDS analysis was performed on samples from the three different engine conditions: low idle, torque stall, and high load. For all cases, the morphology ranged widely, as seen in a typical sample collected on the tenth MOUDI stage, which collects particles with aerodynamic diameters between 56 and 100 nm (Figure 3a).

By observing the morphology of numerous particles with TEM, we identified five types of particles which were distinguished by their morphological and chemical characteristics: (1) agglomerates, (2) optically dense spheres, (3) optically less-dense spheres, (4) core-shell particles, and (5) nanoparticles.

**3.4. Particle Elemental Chemical Composition.** EDS analysis determined the elemental chemical composition of the five common particle types identified by the TEM analysis. The EDS spectra varied from particle to particle, but there were apparent trends. To elucidate these trends and better classify the particle types, a method was designed to qualitatively tabulate the relative abundance of the elements in each spectrum. The method is a simple empirical rating of the intensity of the spectral X-ray peaks of the detected elements. This method was chosen because, when using EDS, it is difficult to obtain accurate quantitative analyses (e.g., percentage composition by weight of particles of varying sizes, morphologies, densities, and elemental composition) without appropriate standards for the elements of interest.

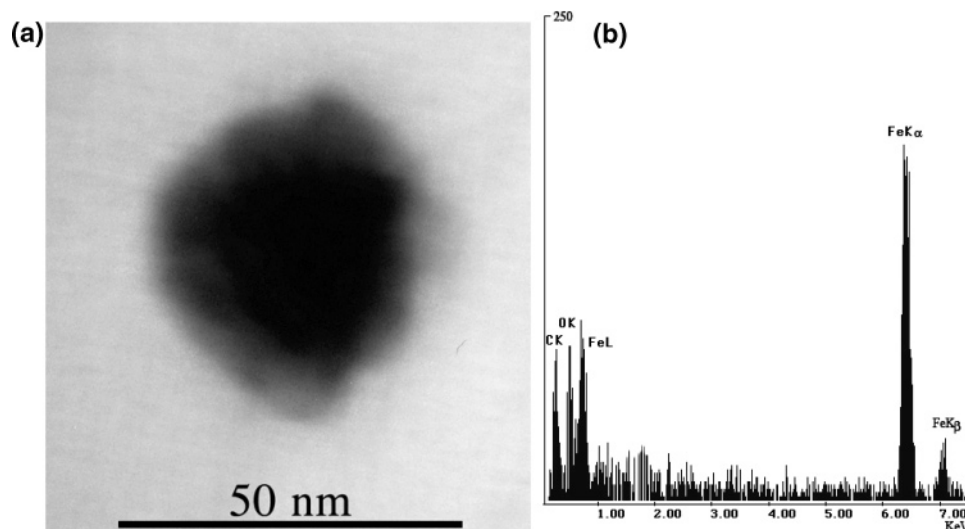


FIGURE 8. Nanoparticle: (a) TEM image and (b) EDS spectrum showing C and Fe peaks.

TABLE 2. Summary of Certified ICP Analysis of the Main Metals Present in the Lubrication Oil

metal	concentration (ppm)
iron	19
lead	6
copper	18
silicon	6
sodium	7
boron	32
zinc	877
phosphorus	1118
calcium	1871
magnesium	72
molybdenum	5

Each particle analysis relied on standardized TEM operating conditions. The spectral peak intensities (peak heights or X-ray counts) above local background per 60 s analysis time were assigned one of four values. Each was judged to be trace (0–25 counts), low (25–50), medium (50–100), or high (>100) and then assigned a value of 1, 2, 3, or 4, respectively. Count values were determined by inspecting each spectrum on the EDS system monitor immediately after acquisition. The count values were tabulated, and the EDS spectra and photographic images of representative particles were recorded. In each morphological class, the count values for each element were summed and divided by the number of particles in that class to yield an average peak intensity value ranging from 0 to 4 for each element. The values were then plotted on a bar graph representing the average rated spectrum (ARS) observed for each morphological class (Figure 3b). Sixty-four particles were included in this tabulation: 23 agglomerates, 10 core-shell spheres, 17 less-dense spheres, and 14 dense spheres. The “nano”-type particles were omitted from Figure 3b because of the difficulty in detection/speciation caused by their small mass. Many of the most common metal species in the averaged rated spectra (Figure 3b) were also evident in the analysis of the lubrication oil (Table 2). This strongly suggests that these particles were derived from the lubrication oil.

**3.5. Detailed Descriptions of Particle Types.** The following sections provide detailed descriptions of identifiable particle types based on the TEM/EDS analysis. For all of the EDS spectra shown in the following figures, the Si and O peaks originating from the support film were removed by subtraction of a spectrum taken from the SiO film (normalized

to each spectra’s Si peak), and any residual O is assumed to be from the particle. The copper peaks produced from the support grid by electron scattering were likewise subtracted from particle spectra.

**3.5.1. Agglomerates.** EDS analysis showed that typical agglomerate particles (Figure 4) were mainly carbonaceous and often had traces of elements such as Na, P, K, S, Sn, Fe, and Zn. The particles of this type were in the 100–400 nm size range. The morphology and elemental composition of these particles bear resemblance to diesel soot (5), suggesting that they are derived in part from the agglomeration of primary particles of EC (soot). Such particles were infrequent in the aerosol from the hydrogen-fueled engine, in contrast to diesel engine combustion, where they are by far the most common particle type (6).

**3.5.2. Dense Spheres.** Spherical particles in the size range of about 30–300 nm (Figure 5) were observed frequently. The spheres appeared very dark in TEM images because of their high density, which mainly consisted of metals, as indicated by the spectrum in Figure 5b. The metals were typically of the kind derived from lubrication oil, that is, Ca, P, Zn, and Mg (Table 2). The high density is likely caused by the Ca content, which is large compared to the signal obtained from less-dense spheres described in section 3.5.3. The dense spherical particles are likely created from lubrication oil constituents, but the particle formation pathway is unclear. One possibility is that they are residue particles created from unburned oil droplets heated enough to evaporate most of the hydrocarbon species. Another possibility is that they contain cores of self-nucleated nonvolatile species, like Fe and Ca, coated with other more volatile species which adsorbed or condensed onto surfaces as the combustion products cooled in the exhaust manifold.

**3.5.3. Less-Dense Spheres.** Particle spheres with a lower optical density than those described in the previous section were also commonly observed (Figure 6). These particles were similar in shape and size to the optically dense particles but appeared to be lighter in color in the TEM image, which suggests more transmission of the electron beam through the particle during imaging. The EDS spectra illustrated that these particles contained metals from the lubrication oil, similar to the more-dense spheres discussed previously. However, the less-dense spheres had a noticeably lower Ca content, which may have contributed to the apparent lower density. It is also notable that many of these particles contained extremely small “nuggets” of dense material.

3.5.4. *Core-Shell Particles*. Some particles were composed of a dense core, high in Fe, Ca, or both, surrounded by a less-dense shell (Figure 7). This suggests that the particles may have formed when vaporized oil residue condensed onto previously nucleated cores as the exhaust gases cooled in the expansion stroke or the exhaust system. This is supported by the observation that the halo around the particle in Figure 7a was susceptible to vaporization upon interaction with the electron beam. The EDS analysis indicated that the lower-density material surrounding such cores was relatively high in the lighter elements derived from lube oil additives (P, K, Mg, Zn, Na), while the cores were generally high in Fe or Ca.

3.5.5. *Nanoparticles*. Particles ranging in size from 5 to 50 nm were classified as nanoparticles. The nanoparticles observed were usually spherical (Figure 8) and composed mainly of Fe (Figure 8b) or a combination of C and Fe. The Fe-rich nanoparticles likely self-nucleated early in the post-combustion process while the temperature was still high. The more carbonaceous nanoparticles likely originate from homogeneous nucleation of volatile hydrocarbon vapors as they exit the engine. These processes have been investigated and described in detail elsewhere (11).

3.6. *Particle-Formation Pathways*. The preceding identification and description of five prevalent types of particles supports the hypothesis that elements dissociated from the lubrication oil during combustion experience a time-dependent gas-to-particle conversion. After initial combustion and during piston retraction, the various vaporized elements undergo nucleation or vapor deposition depending on their volatility, concentration, and the local instantaneous cooling rate. Such a process would likely begin with gas-to-particle conversion of pure (elemental) carbon vapors during the passing of the combustion flame front. There was evidence of a separate nucleation event for the lower volatility metallic vapors of iron and calcium, probably occurring relatively early in the combustion process, suggested by the significant coatings of higher volatility species around iron and calcium cores. For most particles, the metal-to-carbon ratios were higher than for those emitted by other internal combustion engines. This was expected because the combustion of hydrogen does not produce carbon, although some carbon is available from the lubrication oil.

Next, adsorption, condensation, and potentially, further nucleation of metals with higher vapor pressure would occur, in addition to the conversion of the low-volatility hydrocarbons. The more volatile hydrocarbons likely remain in vapor form until after piston retraction, when they begin condensing onto particle surfaces or nucleating homogeneously when the exhaust aerosol cools suddenly during the dilution process. Results of this work imply that new engine technologies that reduce soot levels in the engine or include trace metals in the fuel, may increase both the metal-to-carbon ratio of emitted particles and the generation of metal-rich nanoparticles via self-nucleation. The source of metals for such particle generation could be from fuel impurities, lubrication oil consumption, metals derived from engine wear, or metal-containing fuel additives. Because of their small size and thus efficient lung penetration, the generation of such metallic nanoparticles may introduce health concerns.

## Acknowledgments

The authors thank NIOSH employees Rich Rains, Brian Stapleton, and Patrick Hintz for their assistance in conducting this research. Additional thanks goes to the Seattle University Summer Faculty Fellowship for supporting this work. The findings in this work are those of the authors and do not necessarily represent the views of the National Institute for Occupational Safety and Health (NIOSH). The mention of

specific products and manufacturers does not imply endorsement by NIOSH.

## Literature Cited

- (1) Pope, C. A.; Thun, M. J.; Namboodiri, M. M.; Dockery, D. W.; Evans, J. S.; Speizer, F. E.; Health, C. W. Particulate air pollution as a predictor of mortality in a prospective study of U.S. adults. *Am. J. Respir. Crit. Care Med.* **1995**, *151*, 669–674.
- (2) Utell, M. J.; Frampton, M. W. Acute health effects of ambient air pollution: The ultra-fine particle hypothesis. *J. Aerosol Med.* **2000**, *13*, 355–359.
- (3) Aust, A. E.; Ball, J. C.; Hu, A. A.; Lighty, J. S.; Smith, K. R.; Straccia, A. M.; Veranth, J. M.; Young, W. C. *Particle Characteristics Responsible for Effects on Human Lung Epithelial Cells*; Report 110; Health Effects Institute: Location, 2002; p 65.
- (4) Ghio, A. G.; Richards, J. H.; Carter, J. D.; Madden, M. C. Accumulation of iron in the rat lung after tracheal instillation of diesel particles. *Toxicol. Pathol.* **2000**, *28*, 619–627.
- (5) Lee, D. G.; Miller, A. L.; Park, K.; Zachariah, M. R. Effects of trace metals on particulate matter formation in a diesel engine: Metal contents from ferrocene and lube oil. *Int. J. Automot. Technol.* **2006**, *7*, 667–673.
- (6) Miller, A.; Ahlstrand, G.; Kittelson, D. B.; Zachariah, M. R. The fate of metal (Fe) during diesel combustion: Morphology, chemistry, and formation pathways of nanoparticles. *Combust. Flame* **2007**, *149*, 129–143.
- (7) Flynn, P.; Durrett, R.; Hunter, G.; Loye, A.; Akinyemi, O.; Dec, J.; Westbrook, C. Diesel combustion: An integral view combining laser diagnostics, chemical kinetics, and empirical validation. *SAE Tech. Pap. Ser.* **1999**, 1999-01-0509.
- (8) Siegmann, K.; Sattler, K.; Siegmann, H. C. Clustering at high temperatures: Carbon formation in combustion. *J. Electron Spectrosc.* **2002**, *126*, 191–202.
- (9) Lee, D. G.; Miller, A. L.; Kittelson, D. B.; Zachariah, M. R.; Characterization of metal-bearing diesel nanoparticles using single particle mass spectrometry. *J. Aerosol Sci.* **2005**, *37*, 88–110.
- (10) Skillas, G.; Qian, Z.; Baltensperger, U.; Matter, U.; Burtscher, H. Influence of additives on the size distribution and composition of particles produced by diesel engines. *Combust. Sci. Technol.* **2000**, *154*, 259–273.
- (11) Sakurai, H.; Tobias, H. J.; Park, K.; Zarling, D.; Docherty, K. S.; Kittelson, D. B.; McMurry, P. H.; Ziemann, P. J. On-line measurements of diesel nanoparticle composition and volatility. *Atmos. Environ.* **2003**, *37*, 1199–1210.
- (12) Barris, M. A.; Reinhart, S. B.; Wahlquist, F. H. The influence of lubricating oil and diesel fuel on ash accumulation in an exhaust particulate trap. *SAE Tech. Pap. Ser.* **1991**, 910131, 19–28.
- (13) De Petris, C.; Giglio, V.; Police, G. Some insights on mechanisms of oil consumption. *SAE Tech. Pap. Ser.* **1996**, 961216.
- (14) Bugarski, A. D. Characterization of particulate matter and hydrocarbon emissions from in-use heavy-duty diesel engines. Ph.D. Thesis, Mechanical Engineering, West Virginia University, 1999.
- (15) Okada, S.; Kweon, C.; Stetter, J.; Foster, D.; Shafer, M.; Christensen, G.; Schauer, J.; Schmidt, A.; Silverberg, A.; Gross, D. Measurement of trace metal composition in diesel engine particulate and its potential for determining oil consumption. *SAE Tech. Pap. Ser.* **2003**, 2003-01-0076.
- (16) Jung, H.; Kittelson, D. B.; Zachariah, M. R. The influence of a cerium additive on ultrafine diesel particulate emissions and kinetics of oxidation. *Combust. Flame* **2005**, *142*, 276–288.
- (17) Diesel Particulate Matter Exposure of Underground Metal and Nonmetal Miners. Federal Register 66:13 (19 January 2001), 5706–5755.
- (18) Diesel Particulate Matter Exposure of Underground Metal and Nonmetal Miners. Emission Limits for Nonpermissible Heavy-duty Diesel-powered Equipment, Generators, and Compressors. Federal Register 66:98 (21 May 2001), 27864–27866.
- (19) Baker, N.; Houston, L.; Lynch, F.; Olavson, L.; Sandrock, G. A *Clean Internal Combustion Engine for Underground Mining Machinery: A Technical Assessment and Program Plan*; Open-File Report 86-82, NTIS PB 82-244724, EIMCO Mining Mach. Int.; U.S. Bureau of Mines: Minneapolis, MN, 1981; p 219.
- (20) White, L. Hydrogen fuels underground utility vehicle. *Eng. Min. J.* **2004**, 68–70.
- (21) Bugarski, A.; Mischler, S.; Schnakenberg, G. Effects of alternative fuels on concentrations of nanometer and ultrafine particles in underground mines. Presented at the 9th ETH, Conference on Combustion Generated Nanoparticles, Zurich, Switzerland, 2005.

- (22) Woodward, C. Safety Control Systems Used in a Hydrogen-fueled Mine Vehicle. Presented at the Annual Meeting of the Society for Mining, Metallurgy, and Exploration, 2006.
- (23) McGinn, S. *The Relationship Between Diesel Engine Maintenance and Exhaust Emissions*; Technical Report; Noranda Technology Centre, Diesel Emissions Evaluation Program (DEEP): St-Laurent, Quebec, 2000; p 93.
- (24) Spears, M. W. *An Emission-assisted Maintenance Procedure (EAMP) for Diesel-powered Equipmen*; Technical Report 84; Center for Diesel Research, University of Minnesota: St. Paul, MN, 1997.
- (25) Abdul-Khalek, I. S.; Kittelson, D. B.; Brear, F. The influence of dilution conditions on diesel exhaust particle size distribution measurements. *SAE Tech. Pap. Ser.* **1999**, 1999-01-1142.
- (26) Tamm, H.; Mirme, A.; Tamm, E. Electrical aerosol spectrometer of Tartu University. *J. Aerosol Sci.* **1998**, *29*, S427–S428.
- (27) Birch, M. E. Analytical instrument performance criteria: Occupational monitoring of particulate diesel exhaust by NIOSH Method 5040. *Appl. Occup. Environ. Hyg.* **2002**, *16*, 400–405.
- (28) Cheng, Y. S.; Yeh, H. C.; Kanapilly, G. M. Collection efficiencies of a point to plane electrostatic precipitator. *Am. Ind. Hyg. Assoc. J.* **1981**, *42*, 605–610.
- (29) Roessler, D. M.; Faxvog, F. R.; Stevenson, R.; Smith, G. W. Optical Properties and morphology of particulate carbon: Variation with fuel/air ratio. *Proc. Int. Symp. Particulate Carbon* **1980**, 57–84.
- (30) Zifei, L.; Lu, M.; Birch, M. E.; Keener, T. C.; Khang, S. J.; Liang, F. Variations of the particulate carbon distribution from a nonroad diesel generator. *Environ. Sci. Technol.* **2005**, *39*, 7840–7844.